Intrinsic Uniformity Requirements for Pinhole SPECT

Alain Seret, PhD; and Frédéric Bleeser, BSc

Imagerie Médicale Expérimentale et Centre de Recherche du Cyclotron, Université de Liège, Liège, Belgium

Pinhole SPECT is a fully 3-dimensional tomography technique. Uniformity requirements for γ-cameras have been studied for 2-dimensional SPECT performed with parallel-hole collimators. This study investigated reconstruction artifacts in pinhole SPECT arising from intrinsic uniformity defects of the γ-camera in the case of a pinhole aperture (5 mm) and a rotation radius (10 cm) suitable for human studies. **Methods:** A cylindric phantom was filled with water and ^{99m}Tc. The count density in the pinhole SPECT projections largely exceeded the density that would be expected in human studies. Two-dimensional gaussian-shaped positive uniformity defects of various heights and various full widths at half maximum were simulated at 5 locations on the 64 projections. All these sets of projections were reconstructed using an iterative 3-dimensional ordered-subset expectation maximization (OSEM) algorithm tailored to the pinhole geometry. The influence of the number of OSEM iterations (2, 5, or 8 for 8 subsets) was also investigated. The height of the ring artifacts generated by the uniformity defects was measured on the reconstructed transverse slices and was compared with the noise in the noncorrupted slices. The uniformity defects were also generated on a 30-megacount flood image from the camera. These images were inspected visually, and the National Electrical Manufacturers Association (NEMA) differential and integral uniformities were calculated. **Results:** Defects centered on the line corresponding to the orthogonal projection of the camera axis of rotation onto the detector plane generated artifacts whose magnitude-to-noise ratio exceeded 1% when the defect height was larger than 5%−10%, depending on the defect full width at half maximum. These defects were clearly visible on the slices and the flood images. Defects located elsewhere on the camera detector generated ring artifacts of magnitude-to-noise ratio smaller than 1%. They were visually observable both on the reconstructed slices and on the flood images for defect heights larger than 5%. The increase in the number of OSEM iterations conducted to a decrease in the artifact magnitude-to-noise ratio. **Conclusion:** Although hardly visible on the flood images and only slightly increasing the NEMA differential or integral uniformity, a detector uniformity defect of 3% height is able to generate a visible artifact on the reconstructed transverse slices. The study was conducted on a relatively high-count pinhole SPECT acquisition. Considering that far fewer counts would accumulate in clinical practice, any camera that fulfils these uniformity requirements should not lead to the presence of visible uniformity artifacts in the reconstructed slices.

Received Jul. 16, 2005; revision accepted Nov. 21, 2005.

For correspondence contact: Alain Seret, PhD, Université de Liège, Imagerie Médicale Expérimentale, Institut de Physique, B5, B-4000 Liège1, Belgium.

E-mail: aseret@ulg.ac.be

Key Words: pinhole; SPECT; tomography; uniformity

J Nucl Med Technol 2006; 34:43–47

Several recent studies have highlighted the potential clinical role of pinhole SPECT for the scintigraphic exploration of small organs or of small regions of interest such as the thyroid, the parathyroid glands, the breasts, the shoulder, or the foot joints (*1–7*). The main advantage of pinhole SPECT is a gain in resolution. The smaller the pinhole aperture, the larger is the gain in resolution but the smaller is the sensitivity. This trade-off between resolution and sensitivity limits the choice of aperture size. For human studies, apertures of 4- to 6-mm diameter are generally used (*1–7*). The gain in resolution also depends strongly on the distance between the target region and the pinhole aperture (*1*). To minimize this distance, noncircular orbits and orbits of 180° or even less, combined with tilting of the camera head, have been proposed for the acquisition of projections (*1,2,4–8*). Pinhole SPECT is a fully 3-dimensional (3D) tomography method, regardless of the acquisition scheme (*1,2,4,6–11*).

Quality control procedures for γ-cameras have been developed mainly for use with parallel-hole collimators. Some of these procedures should be reconsidered when a pinhole collimator is used for SPECT. The requirements for center-of-rotation stability are high for pinhole SPECT and have been studied in detail (*10*). The detector uniformity of response is also important for SPECT performed with a rotating camera. It has been clearly shown that the uniformity requirements are much more stringent for SPECT with parallel-hole collimators than for planar imaging (*12–14*). However, SPECT images obtained with parallel-hole collimators are usually reconstructed with a 2-dimensional (2D) algorithm. In contrast, pinhole SPECT requires the use of a 3D algorithm (*1,2,4,6–11*).

The present study quantitatively analyzed the reconstruction artifacts resulting from detector uniformity defects of different magnitudes and sizes in a SPECT pinhole study. To avoid the limitations and the additional nonuniformity due to incomplete trajectories (*6–8*), we used a full 360° acquisition. The pinhole aperture size (5 mm) and the rotation radius (10 cm) were chosen to represent typical

clinical conditions. The reconstruction was performed with a 3D ordered-subset expectation maximization (OSEM) dedicated algorithm, because iterative reconstruction methods have been shown to deliver images of higher clinical quality (*4,9,11*).

MATERIALS AND METHODS

Materials

The pinhole SPECT acquisitions were performed using a Sophy DSX camera (SMV International) fitted with a pinhole collimator 205 mm tall, with a 295-mm-diameter circular base and a 5-mm-diameter aperture. The camera head was not tilted in this study. The energy window was centered at 140 keV with a total width of 20%, and 64 projections over 360° were acquired using a circular orbit of 100-mm radius. The projection pixel size was 2.75 × 2.75 mm (128 × 128 matrix and a hardware zoom of 2.0). A 250-mL laboratory bottle of 58-mm inner diameter and filled with an aqueous solution of 375 MBq of ^{99m}Tc served as a uniformity phantom. It was positioned with its central axis parallel and close (within 5 mm) to the axis of rotation. A mean of 275 kcts per projection were accumulated for a total of 17.6 megacounts (Mcts).

A ^{99m}Tc point source at a distance approximately 6 times the largest field of view of the camera was used to obtain a 30-Mct uniformity image (flood image) in a 128 × 128 matrix. Analysis of this flood image with the National Electrical Manufacturers Association (NEMA) software package of the camera resulted in an integral uniformity of less than 2% and a differential uniformity of 1.5% in the useful field of view.

Methods

Various uniformity defects were added to the projections at 5 locations (Fig. 1) by multiplying the projections by a positive 2D gaussian function. The height of the gaussian (defect height) was varied between 0% and 50%; the width of the gaussian (defect full width at half maximum [FWHM]) was 5, 10, 15, or 20 pixels FWHM. To evaluate the impact of some defects on the quality control results for the intrinsic uniformity of the camera, we used the same procedure to generate uniformity defects on the flood image. These flood images with uniformity defects were then exported to the computer of the camera and analyzed using the NEMA software package of the camera.

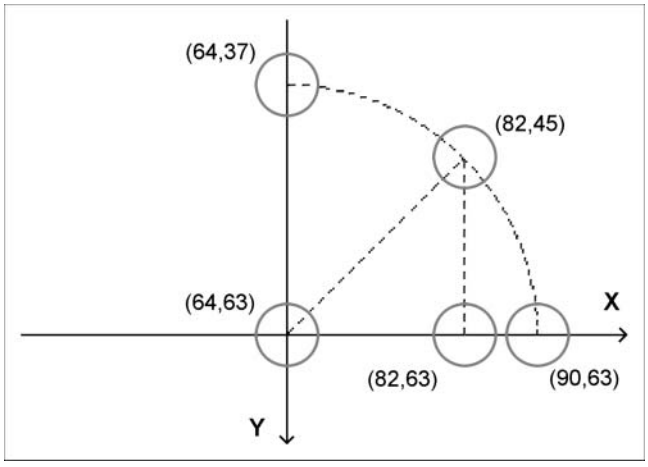

FIGURE 1. Location of center of defects that were simulated on projection images (128 × 128 matrix) of SPECT uniformity phantom. *y*-axis corresponds to orthogonal projection of camera axis of rotation onto detector plane.

OSEM reconstruction software tailored to pinhole geometry was used to obtain 128 transverse slices in the 128 × 128 matrix (*6,8*). Eight subsets were used throughout the study, with 2, 5, or 8 iterations. The files containing the reconstructed slices were then transferred to a personal computer. These images were subsequently analyzed using Image software (Scion Corp.).

Analysis of Results

The noise in reconstructed slices was evaluated from reconstructions of the original projections without any added defect. The SD and mean pixel value of each transverse slice were obtained from a large, circular region of interest inside the uniform section of the phantom. The ratio of the SD to the mean pixel value was converted to a percentage, rounded to an integer, and expressed as the percentage root mean square (%RMS) of noise in the slice.

The uniformity defects resulted in a disk or ring artifact on some reconstructed transverse slices. The artifact was always greatest on the transverse slice corresponding to the *y*-coordinate of the defect. Two orthogonal profiles intersecting at the slice center were drawn on this slice. Each profile resulted in 1 (disk artifact) or 2 (ring artifact) maxima. The magnitude of the maxima from the 2 profiles (2 maxima for a disk, 4 maxima for a ring) were averaged and taken as the artifact magnitude.

One of us visually analyzed the reconstructed transverse slices. For each defect location and each defect FWHM, the slices were examined in order of decreasing defect height. The starting point was always 50% of the defect height so that the location and shape of the artifact on the reconstructed slices could be determined. The minimum defect height that generated a visually observable artifact was noted.

RESULTS

The %RMS for noise in the reconstructed slices increased with the number of OSEM iterations: 18%, 36%, and 50% for 2, 5, and 8 iterations, respectively.

In the reconstructed transverse slices, defects at the level ($x = 64$) of the orthogonal projection of the rotation axis onto the detector plane resulted in disk artifacts, whereas other defects ($x = 82$ or 90) resulted in ring artifacts, as shown in Figure 2. The ratio of artifact magnitude to %RMS is plotted against defect height in Figure 3 for the 4 defects studied. The effect of the number of OSEM iterations on this ratio is plotted in Figure 4 for defects of 5 pixels FWHM. Similar behavior was seen for larger defects.

From the visual analysis, a minimum defect height of 3% was required to generate a visually observable artifact on the reconstructed transverse slices. This threshold was obtained for a defect of 5 pixels FWHM centered on the line corresponding to the orthogonal projection of the rotation axis onto the detector plane ($x = 64$). All other defect locations or widths yielded a minimum defect height that exceeded 5%.

The NEMA differential uniformity did not change for defects of 3% or 5% height generated on the flood image. For a defect of 5 pixels FWHM, the NEMA integral

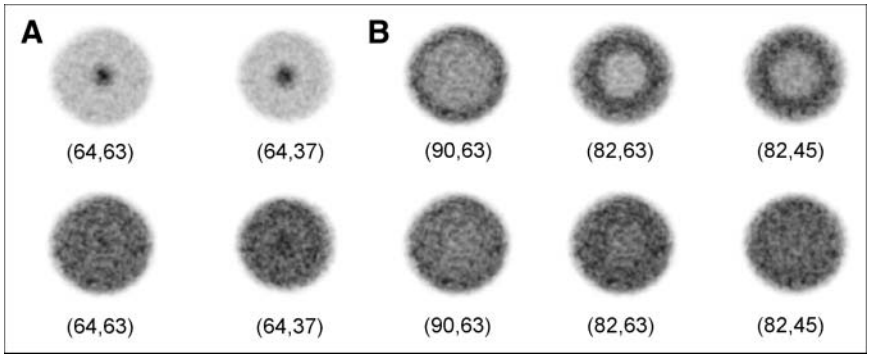

FIGURE 2. Reconstructed transverse slice for defect of 50% height (top) and of minimum height that still generates visible artifact (bottom) for defects centered on line corresponding to orthogonal projection of camera axis of rotation onto detector plane ($x = 64$) (A) and for defects located elsewhere ($x = 82$ or 90) (B).

uniformity did not change for 3% defect height and increased slightly from 2% to 2.3% for 5% defect height. The defect of 3% height was hardly visible on the flood image (Fig. 5) even from the computer screen and when using the blue-yellow (hot iron) color scale. Larger defects of 3% height were more clearly visible but still resulted in slight increases in NEMA integral uniformity. For example, a defect of 3% height and 15 pixels FHWM resulted in a 2.28% value instead of the 2% value for the original flood image without a simulated defect. Finally, defects higher than 5% were more easily seen on the flood image regardless of their FWHM (Fig. 5).

DISCUSSION

Advances in camera hardware, essentially in center-of-rotation stability, and in 3D reconstruction algorithms have made pinhole SPECT available to routine clinical practice. In comparison with SPECT performed with parallel-hole collimators, the main advantage is an improved resolution and the major disadvantages are a limited field of view and a sometimes-reduced sensitivity. Although not widely used, pinhole SPECT has some potential for scintigraphic exploration of small bones (*3,6*) or of small organs such as the thyroid (*1,4*) or the parathyroid glands (*5*).

Pinhole SPECT is a fully 3D tomography technique (*9,10*). Uniformity requirements for SPECT cameras have been established mainly from studies performed with parallel-hole collimators and 2D (either filtered backprojection or iterative OSEM) reconstruction methods (*12–14*). The validity of these criteria for pinhole SPECT can therefore be questioned.

We addressed this problem starting from a high-count pinhole SPECT study of a uniform cylindric phantom. The density of accumulated counts in the projections was higher than could be obtained during examination of a patient (*6*). Incomplete (less than 360°) orbits and even a tilted camera head are required for most human examinations (*1,6,7*). However, such orbits lead to artifacts in some area of the reconstructed slices (*6*). Therefore, a complete (360°) orbit and no detector tilt were used to acquire the projection data. The visibility of uniformity artifacts is highly dependent on image noise (*12,14*), and the reconstruction algorithm affects this noise. OSEM is used to reconstruct the data because OSEM is superior to filtered backprojection for pinhole SPECT (*9*).

The increase of noise in reconstructed slices as the number of OSEM iterations increases is a well-known phenomenon observed both in 2D (*14*) and in 3D (*11*) OSEM reconstructions. The shape of the artifact generated by a uniformity defect is similar for 2D SPECT (*12–14*) and pinhole SPECT (Fig. 2) when both are acquired with a circular orbit. The artifact looks like a disk for a defect centered on the line corresponding to the orthogonal projection of the axis of rotation onto the detector plane (Fig. 2A) and a ring for a defect located elsewhere on the

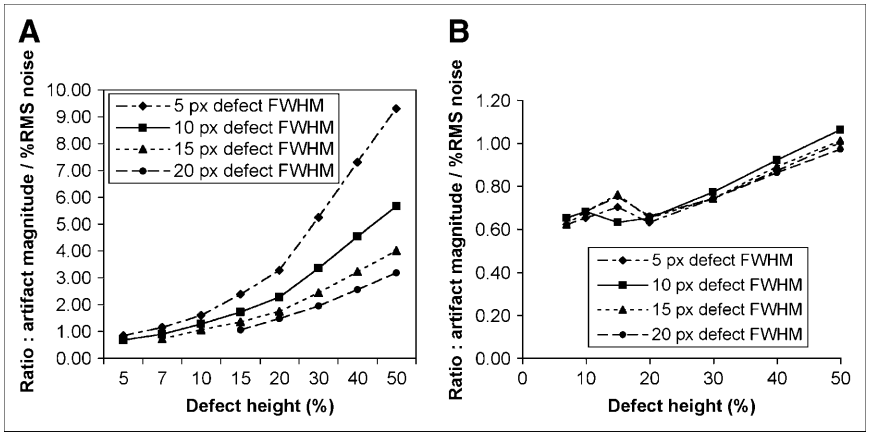

FIGURE 3. Ratio of artifact magnitude to slice noise as function of height of gaussian defect created on projection data for defects centered on line corresponding to orthogonal projection of camera axis of rotation onto detector plane ($x = 64$) (A) and for defects located elsewhere ($x = 82$ or 90) (B). px = pixel.

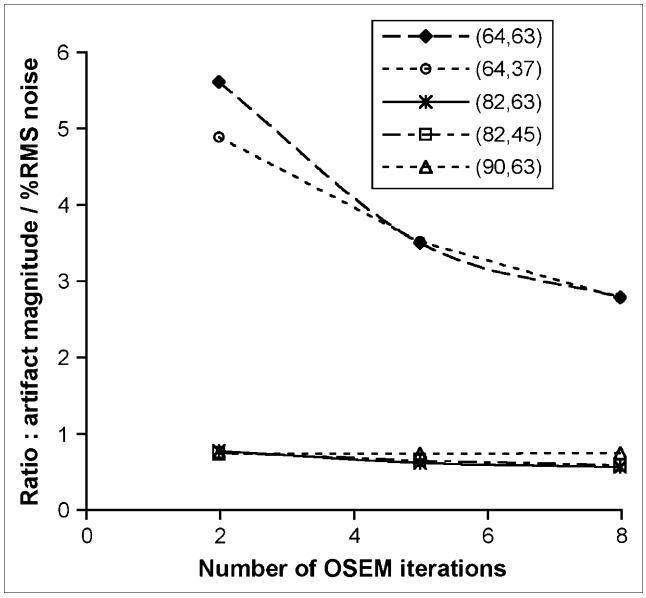

FIGURE 4. Ratio of artifact magnitude to slice noise as function of number of OSEM iterations for defects of 5 pixels FWHM.

detector (Fig. 2B). The magnitude of the artifact increases with the intensity of the defect. This behavior is also observed in 2D SPECT (*14*). For defects not near the line corresponding to the orthogonal projection of the axis of rotation onto the detector plane, the magnitude of the artifact does not depend on defect width (Fig. 3B). The same observation is made for 2D SPECT (*14*). However, when the defect is centered on the line corresponding to the orthogonal projection of the axis of rotation onto the detector plane, artifact magnitude clearly increases as defect width decreases (Fig. 3A). Visual analysis confirms this observation. Indeed, a minimum defect height of 3% has been found to be required to generate a visually observable artifact on reconstructed transverse slices. This threshold is obtained for a defect of 5 pixels FWHM located on the rotation axis; all other defect widths lead to a larger minimum defect height.

Artifact magnitude increases with the number of OSEM iterations. However, noise in the reconstructed slices increases more rapidly, and the ratio of artifact magnitude to %RMS decreases for most defect locations ($x = 64$ or 82) or remains nearly unchanged ($x = 90$). The $x = 90$ defects form a ring artifact near the border of the reconstructed bottle image. A difference in OSEM convergence for this area might explain the difference in the behavior of this defect. Leong et al. (*14*) reported, for 2D SPECT, an increase in the ratio of artifact magnitude to %RMS for defects near the orthogonal projection of the rotation axis onto the detector plane and a decrease in this ratio for defects farther from this projection line when the number of OSEM iterations increased.

Visual analysis showed that a defect with a height as low as 3% and centered on the orthogonal projection of the rotation axis onto the detector plane can generate a visible artifact on reconstructed slices. The impact of such a defect on routine quality control of the uniformity of the camera is studied by generating this defect on a high-count (30 Mcts) flood image from the camera. The 3% defect height does not change the NEMA integral uniformity. A 5% defect height modified this NEMA parameter from 2% to 2.3%. Such a low change would probably not be taken as significant. However, these defects were visible on the flood image. We therefore recommend not only that the NEMA parameters be analyzed but also that the flood image be critically observed, especially in the area of the orthogonal projection of the axis of rotation onto the detector plane. In this study, high-count SPECT was used, and the human observer knew the shape of the artifact and its location on the reconstructed slices. Therefore, the minimum defect height and width that would generate an observable artifact were larger under clinical conditions. Such defects should be more easily detected on flood images obtained for quality control of uniformity.

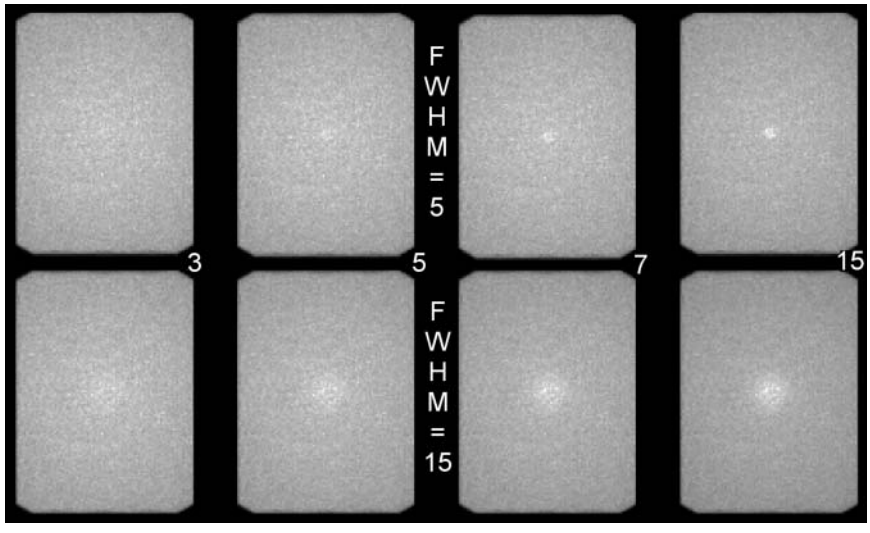

FIGURE 5. Flood uniformity image (30 Mcts) with simulated gaussian defect of 5 (top) or 15 (bottom) pixels FWHM. Defect height is 3%, 5%, 7%, and 10%, from left to right. Nonlinear (γ, 0.5) gray scale is used. The 4 defects are more clearly visible on camera screen, particularly with blue-yellow (hot iron) color scale.

The present study was limited to acquisition parameters convenient for pinhole SPECT of humans, and the conclusions should therefore not be extrapolated to other acquisition parameters. This is particularly true for small-animal studies in which the pinhole aperture and the rotation radius are smaller and in which a higher number of counts can potentially accumulate.

CONCLUSION

Although hardly visible on the flood images and only slightly increasing the NEMA differential or integral uniformity, a detector uniformity defect of 3% height can generate a visible artifact on reconstructed transverse slices. This study was conducted on a relatively high-count pinhole SPECT acquisition. Considering that far fewer counts would accumulate in clinical practice, any camera that fulfils these uniformity requirements should not lead to uniformity artifacts in the reconstructed slices.

REFERENCES

1. Wanet PM, Sand A, Abramovici J. Physical and clinical evaluation of high-resolution thyroid pinhole tomography. *J Nucl Med.* 1996;37:2017–2020.
2. Scarfone C, Jaszczak RJ, Li J, et al. Breast tumour imaging using incomplete circular orbit pinhole SPET: a phantom study. *Nucl Med Commun.* 1997; 18:1077–1086.
3. Bahk YW, Chung SK, Park YH, Kim SH, Lee HK. Pinhole SPECT imaging in normal and morbid ankles. *J Nucl Med.* 1998;39:130–139.
4. Desvignes P, Laurette I, Koulibaly PM, Migneco O, Bussière F, Darcourt J. An algebraic 3D reconstruction method for pinhole SPECT: validation for cold thyroid nodule detection [abstract]. *Eur J Nucl Med.* 2000;27:942.
5. Gabriel M, Erler H, Profanter C, Moncayo R, Riccabona G. Evaluation of parathyroid nodules with thallium/technetium pinhole SPECT [abstract]. *Eur J Nucl Med.* 2000;27:1070.
6. Seret A, Defrise M, Blocklet D. 180 degree pinhole SPET with a tilted detector and OS-EM reconstruction: phantom studies and potential clinical applications. *Eur J Nucl Med.* 2001;28:1836–1841.
7. Tornai MP, Bowsher JE, Jaszczak RJ, et al. Mammotomography with pinhole incomplete circular orbit SPECT. *J Nucl Med.* 2003;44:583–593.
8. Seret A, Flérès D, Firket O, Defrise M. Body contour 180 degrees pinhole SPET with or without tilted detector: a phantom study. *Eur J Nucl Med Mol Imaging.* 2003;30:1205–1210.
9. Vanhove C, Defrise M, Franken PR, Everaert H, Deconinck F, Bossuyt A. Interest of the ordered expectation maximisation (OS-EM) algorithm in pinhole single-photon emission tomography reconstruction: a phantom study. *Eur J Nucl Med.* 2000;27:140–146.
10. Li J, Jaszczak RJ, Greer KL, Coleman RE. A filtered-backprojection algorithm for pinhole SPECT with a displaced centre of rotation. *Phys Med Biol.* 1994;39:165–176.
11. Sohlberg A, Kuikka JT, Ruotsalainen U. Pinhole single-photon emission tomography reconstruction based on median root prior. *Eur J Nucl Med Mol Imaging.* 2003;30:217–221.
12. Rogers WL, Clinthorne NH, Harkness BA, Koral KF, Keyes JW. Field-flood requirements for emission computed tomography with an Anger camera. *J Nucl Med.* 1982;23:162–168.
13. Gullberg GT. An analytical approach to quantify uniformity artifacts for circular and noncircular detector motion in single photon emission computed tomography imaging. *Med Phys.* 1987;14:105–114.
14. Leong LK, Kruger RL, O'Connor MK. A comparison of the uniformity requirements for SPECT image reconstruction using FBP and OSEM techniques. *J Nucl Med Technol.* 2001;29:79–83.